

Wall Effect on A Spherical Particle Settling along The Axis of Cylindrical Tubes Filled with Carreau Model Fluids

Daoyun Song^{*1}, Rakesh K. Gupta¹, and Rajendra P. Chhabra²

¹West Virginia University, ²Indian Institute of Technology, Kanpur, India

*Corresponding author: Department of Chemical Engineering, West Virginia University, PO Box 6102, Morgantown, WV 26506, dysong@gmail.com

Abstract: The effect of finite boundaries on the drag experienced by a rigid sphere settling along the axis of cylindrical tubes filled with Carreau model fluids has been examined systematically. Specifically, the governing equations along with the boundary conditions were numerically solved over a wide range of conditions, sphere-to-tube diameter ratio: 0-0.5; Reynolds number: 1-100; Carreau number: 0.1-100; and power law index: 0.2-1. As expected, the presence of finite boundaries leads to an increase in the drag force exerted on a falling sphere thereby retarding its descent due to the obstruction caused by the sphere and the corresponding changes in the velocity field close to the sphere. Nonetheless, the wall effect is less significant as the power law index decreases and/or the Carreau number increases, i.e., increasing extent of shear-thinning behavior. Besides the impact on the hydrodynamic drag, the severity of bonding walls affects the wake characteristics. The present calculations show good agreement with experimental reports available in the literature.

Keyword: Wall effect, Carreau model, terminal falling velocity, creeping region, shear-thinning fluids

1. Introduction

The flow of non-Newtonian fluids past a rigid sphere has a broad range of practical applications such as gravity-based separation techniques employed in processing of chemical, mineral suspensions and foodstuffs, and flow in fixed, fluidized and multiphase fluidized bed reactors. A thorough understanding of the hydrodynamic behavior of a spherical particle is beneficial for developing useful insights into the behavior of non-spherical particles and/or their clusters. Over the years, a wealth of literature has addressed the problem of fluid flow and heat transfer past a sphere in an unconfined region, especially in Newtonian fluids and to a limited extent in power-law fluids. However, the flow

over a sphere in a confined region is encountered in various applications such as falling ball viscometry, hydrodynamic chromatography, membrane transport, and hydraulic transport of coarse solids in pipes. Although several authors have taken into account the finite wall effect on flow, the fluids considered are limited to Newtonian ones. It is worth noting here that many fluids of industrial interest display shear-thinning behavior. Indeed, for most fluids such as polymer melts, polymer solutions, food emulsions, suspensions, and biological fluids the power-law index, n , indicative of shear-thinning degree, is typically in the range of ~ 0.2 and ~ 0.8 .¹ Since the flow of Newtonian and power-law fluids has already been investigated systematically by Song et al.,^{2,3} this work will focus on the flow of Carreau model fluids which takes into account the influence of zero-shear viscosity exhibited by most polymeric fluids at low shear rates. Therefore, the Carreau viscosity model is quite flexible in fitting viscosity data for most systems. When the shear rate approaches zero, it reduces to the Newtonian viscosity law; when the shear rate is large, the well-known power-law model is recovered. Chhabra et al.^{4,5} have experimentally examined the flow of the Carreau model fluids over a sphere. Stradel et al.⁶ numerically studied the wall effect in Carreau fluids over a sphere in the creeping flow regime. Hsu et al.⁷ have investigated the boundary effect of Carreau fluids flow over spherical and non-spherical particulates, but the maximum Reynolds number, Re , is limited to 40, and the minimum power-law index 0.4. This work will thoroughly examine the interplay between the degree of confinement (the ratio of sphere diameter to the tube diameter, $\kappa=d/D$), Carreau number (or dimensionless time) ($\Lambda=\lambda V_0/d$), power-law index, n , and Reynolds number, Re on the hydrodynamics over wide ranges of conditions as: sphere Reynolds number, Re : 1-100, the sphere-to-tube diameter ratio, κ : 0-0.5, and the power law index, n : 0.2-1 and the Carreau number, Λ : 0.1-100.

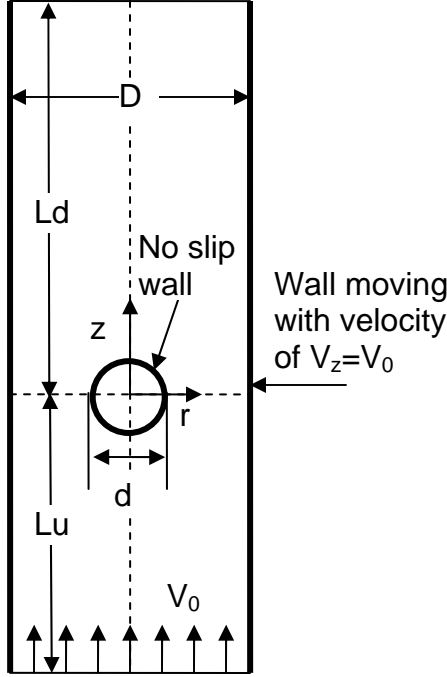


Figure 1. Schematic of flow around a sphere in a cylindrical tube

2. Governing Equations

Consider a scenario in which a sphere with a diameter d located at the axis of a cylindrical tube having a diameter D falls at a steady velocity V_0 in a tube filled with a quiescent liquid (Carreau model). This situation is tantamount to the fluid moving at a uniform velocity of V_0 around the stationary sphere as shown schematically in Figure 1. Notice that the walls also move upwards at the same velocity V_0 .

For a two-dimensional, axisymmetric, steady flow in cylindrical coordinates, the governing equations in their compact forms are written as follows,

$$\text{Continuity equation} \quad \nabla \cdot \mathbf{V} = 0 \quad (1)$$

$$\text{Momentum equation in terms of stress} \quad \rho \mathbf{V} \cdot \nabla \mathbf{V} = -\nabla p + \nabla \cdot \boldsymbol{\tau} \quad (2)$$

where \mathbf{V} is the velocity vector; $\boldsymbol{\tau}$, the extra stress tensor; p , pressure; and ρ , density. A constitutive equation is needed for the problem closure. In this work, the Carreau model is adopted.⁸

The Carreau model can be written as

$$\boldsymbol{\tau} = \eta(|\dot{\boldsymbol{\gamma}}|)\dot{\boldsymbol{\gamma}} \quad (3)$$

in which

$$\eta - \eta_\infty = (\eta_0 - \eta_\infty) \left[1 + (\lambda |\dot{\boldsymbol{\gamma}}|^2)^{n-1} \right]^{1/2},$$

$$|\dot{\boldsymbol{\gamma}}| = \sqrt{\frac{1}{2} \dot{\boldsymbol{\gamma}} : \dot{\boldsymbol{\gamma}}}, \quad \dot{\boldsymbol{\gamma}} = \nabla \mathbf{V} + \nabla \mathbf{V}^T \quad (4)$$

where η_0 and η_∞ are the zero shear rate and infinite shear rate viscosities, respectively; λ is a characteristic time constant, determining the point of onset of shear thinning; n is the power law index in the shear-thinning region; $|\dot{\boldsymbol{\gamma}}|$ is the magnitude of the shear rate tensor, $\dot{\boldsymbol{\gamma}}$.⁸ Notice that usually η_∞ is much smaller than η_0 . Thus, it is neglected here. When the shear rate approaches to zero, the Carreau model reduces to $\eta = \eta_0$ (a Newtonian fluid); while the shear rate is large, i.e., $\lambda |\dot{\boldsymbol{\gamma}}| \gg 1$, the well-known power-law model is recovered,

$$\eta = (\eta_0 \lambda^{n-1}) |\dot{\boldsymbol{\gamma}}|^{n-1} = m |\dot{\boldsymbol{\gamma}}|^{n-1} \quad (5)$$

in which m is the consistency index. Thus, this model is quite flexible in fitting viscosity data for many systems.

The flow curves predicted by the Carreau model are shown in Figure 2. Clearly, at low shear rates, it exhibits Newtonian fluid behavior; whereas at high shear rates, it displays shear-thinning (power-law model) feature, both of which are expected from Eq. (4). When n remains constant (at either 0.6 or 0.2), flow curves shift downwards with the increase of λ . This indicates two things. On the one hand, the viscosity decreases with increasing value of λ ; on the other hand, the onset of shear-thinning behavior shifts towards low shear rates as λ increases.

Boundary conditions for this flow are written as follows,

- (1) Inlet
 $V_r = 0, V_z = V_0$
- (2) Outlet
 $p=0, \partial V_z / \partial z = 0$
- (3) Symmetry
 $V_r = 0$
- (4) Sphere wall
 $V_r = V_z = 0$
- (5) Tube wall
 $V_r = 0, V_z = V_0$

Once the above governing equations along with the associated boundary conditions are numerically solved, the solutions are usually used to deduce values of macroscopic characteristics of interest. Thus, it is useful to introduce some dimensionless parameters like sphere Reynolds number, Re , and drag coefficient, C_D .

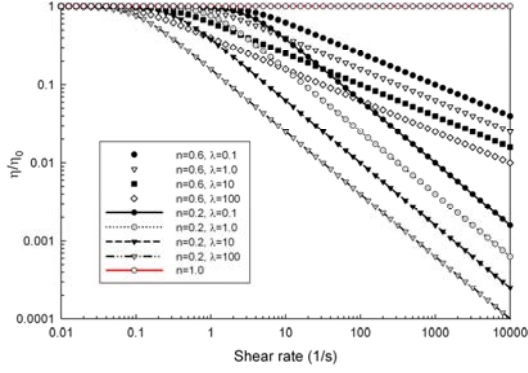


Figure 2. Shear viscosity curves at different n and λ

The sphere Reynolds number, Re , is defined by

$$Re = dV_0\rho/\eta_0 \quad (6)$$

The drag coefficient, C_D , is defined as

$$C_D = \frac{8F_D}{\rho V_0^2 \pi d^2} \quad (7)$$

in which F_D is the total drag force exerted by the fluid on the sphere surface and is calculated from the following equation (n is the normal direction along the sphere surface, and e_z is the unit vector along the flow direction, z -direction here)

$$F_D = \int_{\partial\Omega} [(-pI + \tau) : ne_z] ds \quad (8)$$

The other two dimensionless parameters are the flow behavior index, n and the Carreau number, Λ defined as $\Lambda = \lambda V_0/d$.

3. Use of COMSOL Multiphysics

Since the numerical solution methodology has been described in detail elsewhere,^{2,3} it was briefly recapitulated here. The governing equations together with the appropriate boundary conditions were solved using COMSOL Multiphysics (version 3.5a). The flow geometry was drawn by means of the built-in CAD tools, and the flow domain was meshed using “quadrilateral” elements. The built-in steady-state “Non-Newtonian Flow” module was selected to solve the problem. The scheme of Lagrange- P_2P_1 for velocity and pressure was chosen to handle the velocity-pressure coupling. Once the flow domain was mapped in terms of the velocities, pressure and stresses, global characteristic quantities of interest, such as the drag coefficient, were obtained through post processing.

Certainly, the reliability and accuracy of the numerical solutions are dependent on the choice of domain and mesh. Here, domain is

characterized by the upstream length, Lu and the downstream length, Ld , as shown in Figure 1. Based on extensive experimentation coupled with previous experience,^{2,3} it was found that $Lu=50R$ and $Ld=250R$ are adequate over the range of conditions examined in this study. In order to evaluate wall effect with respect to the unconfined situation, a sphere-in-sphere configuration was employed with the outer sphere radius of $R_\infty=500R$ to mimic this scenario of $\kappa \rightarrow 0$. This value of R_∞ is believed to be sufficiently large to simulate the unbounded situation over the range of Reynolds numbers studied herein. Provided the balance of mesh refinement and computational resource requirements in terms of CPU time and memory, it is believed that meshes comprising 6138 elements for the unconfined case ($\kappa=0$), 12850 elements for $d/D=0.1$, 11710 elements for $d/D=0.2$, 9450 elements for $d/D=0.3$, 9170 elements for $d/D=0.4$ and 9050 elements for $d/D=0.5$, respectively are satisfactory for the purpose of this study.

4. Results and Discussion

In this study, extensive numerical simulations have been carried out for the following ranges of conditions: power law index, $0.2 \leq n \leq 1$; Reynolds number, $1 \leq Re \leq 100$; diameter ratio: $0 \leq \kappa \leq 0.5$ and Carreau number: $0.1 \leq \Lambda \leq 100$. Before presenting our results, it is necessary to establish the reliability and accuracy of present results.

4.1 Comparison with Experiments

Chhabra et al.^{4,5} have experimentally examined the flow of the Carreau model fluids over a sphere in both unconfined and confined scenarios. First, the present calculations are compared with their results in the unbounded case and in the creeping regime.⁴ As shown in Figure 3, the present computations are in good agreement with experimental data. Note that the drag correction factor, X is defined by the following expression,

$$X = \frac{F_D}{6\pi\eta_0 V_\infty R} \quad (9)$$

In addition to the experiments in an unconfined scenario, Chhabra et al.⁵ conducted experiments of sphere freely falling in confined quiescent Carreau fluids in the creeping flow regime, thereby being capable to take into

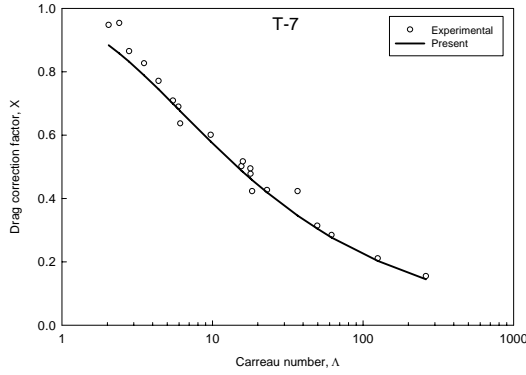


Figure 3. Comparison of drag correction factor of present computations and Chhabra and Uhlherr.⁴

account wall effect. The wall effect of finite boundaries, wall factor, f on sphere sedimentation is expressed in terms of the ratio of the terminal velocity in the confined (arbitrary κ) and unconfined ($\kappa=0$) media, defined as

$$f = \frac{V}{V_\infty} \quad (10)$$

Notice that for a fixed set of experiments (only the diameter ratio of the sphere to the tube varies) in Reference 5, the drag force acting on the sphere remains constant, which equals

$$F_D = \frac{4}{3} \pi R^3 g (\rho_s - \rho_l) \quad (11)$$

Certainly, due to the retardation influence of finite boundaries, V is less than V_∞ . As a result, in each set of experiments, Carreau number is not equal, but $\Lambda < \Lambda_\infty$. Consequently, in the simulation, first select a set of experimental results, and conduct simulations in the unbounded circumstance matching the fluid power law index (n) and the Carreau number (Λ) in the creeping flow region (here $Re=1E-3$); then obtain the total drag force exerting on the sphere followed by simulating the scenarios of arbitrary κ (0.05, 0.1, 0.2, 0.3, 0.4 and 0.5). Under each situation, the velocity is adjusted in such a way that the total drag force matches that in the unconfined case. Figure 4 shows the comparison between the present calculations and one set of experimental data from Reference 5. It is worth mentioning that the experimental values shown in Figure 4 are either interpolated or extrapolated based on the original experimental data in Reference 5. As seen in Figure 4, when the diameter ratio is equal to or less than 0.3, they are in good agreement ($\pm 6\%$); the deviation increases as κ is equal to or greater than 0.4. Overall, the agreement is seen to be satisfactory.

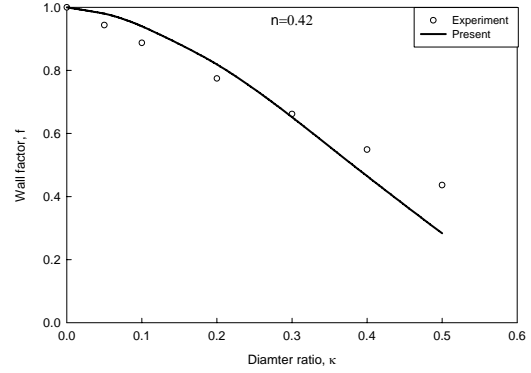
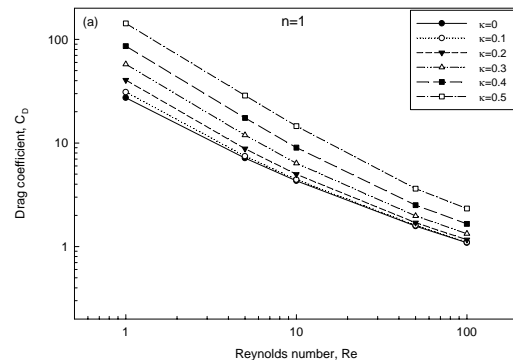


Figure 4. Comparison of wall factor between present predictions and experimental data.⁵

4.2 Effects of Reynolds number, Carreau Number and Diameter Ratio on Drag Coefficient

Figure 5 shows the dependence of drag coefficient on Reynolds number, power law index and diameter ratio at a constant Carreau number of 10. For the purpose of comparison, the unconfined situation corresponding to $\kappa=0$ is also included. As expected, the drag coefficient in the confined case is always larger than that in the unconfined case. In addition, all else being equal, drag increases with the increase of κ . This can be attributed to a steeper velocity gradient near the sphere surface. On the other hand, this effect diminishes gradually with increasing Reynolds number. An examination of Figure 5 also reveals that as n decreases, i.e., increasing shear-thinning behavior, curves at different values of κ tend to come closer, as seen in Figure 5(f) ($n=0.2$). This may be interpreted as follows, with a constant confinement, when n decreases, the effective viscosity decreases due to shear-thinning behavior. The role of confinement at high Reynolds numbers is mitigated mainly due to the increasing significance of inertial influence. As a result, the viscous effect becomes less.^{2,3}



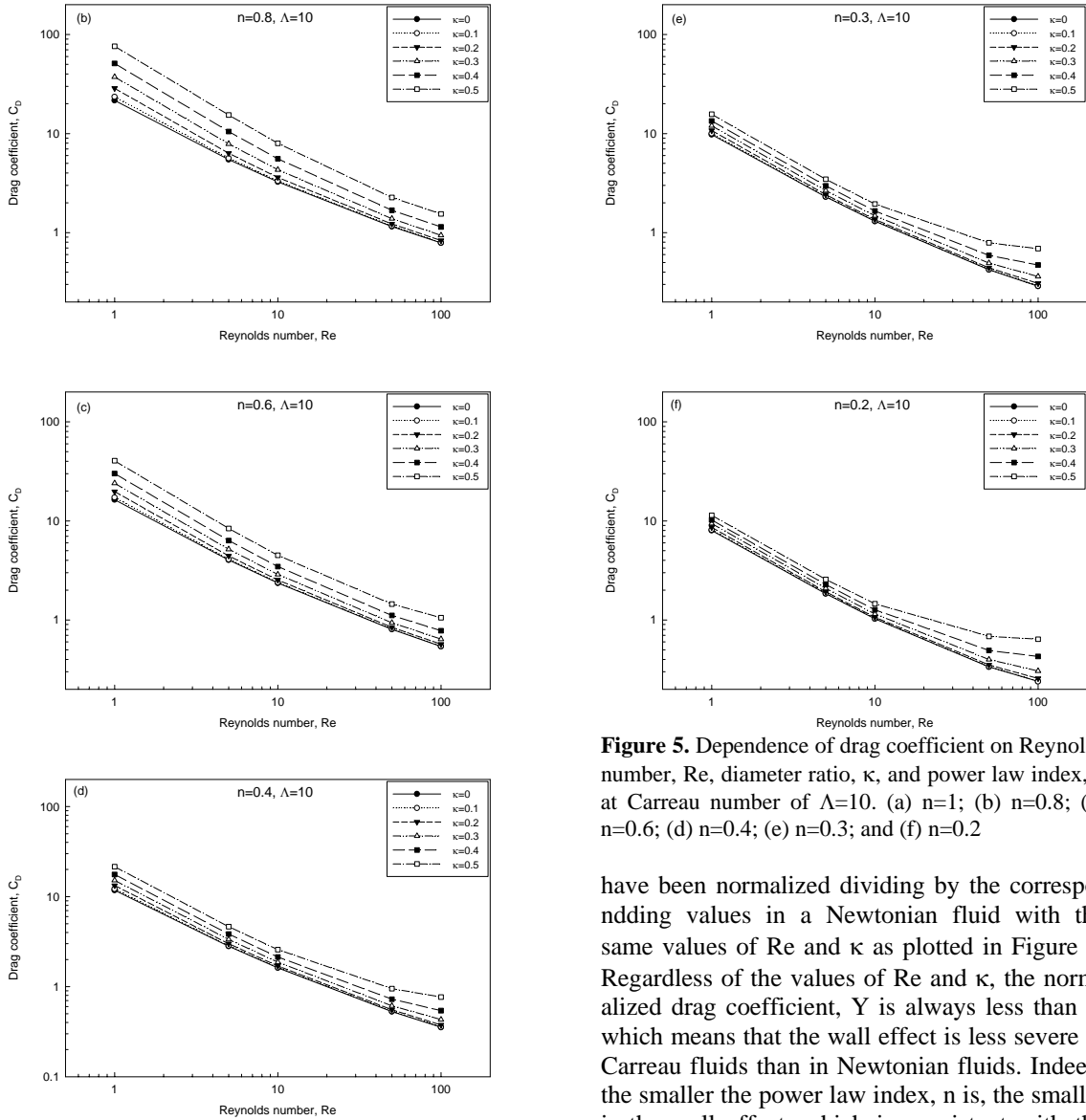
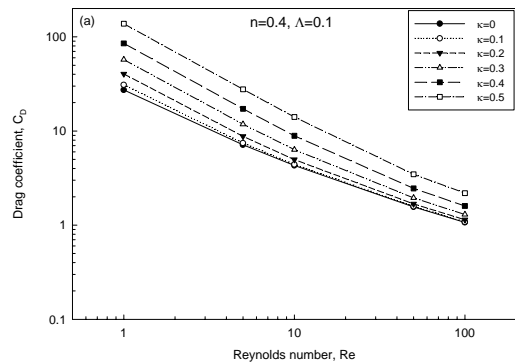


Figure 5. Dependence of drag coefficient on Reynolds number, Re , diameter ratio, κ , and power law index, n at Carreau number of $\Lambda=10$. (a) $n=1$; (b) $n=0.8$; (c) $n=0.6$; (d) $n=0.4$; (e) $n=0.3$; and (f) $n=0.2$

have been normalized dividing by the corresponding values in a Newtonian fluid with the same values of Re and κ as plotted in Figure 7. Regardless of the values of Re and κ , the normalized drag coefficient, Y is always less than 1, which means that the wall effect is less severe in Carreau fluids than in Newtonian fluids. Indeed, the smaller the power law index, n is, the smaller is the wall effect, which is consistent with the case of sphere falling in power-law fluids.^{2,3} Aside from the above, this effect is enhanced with the increase of κ and/or the decrease of Re , qualitatively similar to the case of power-law

So far, the Carreau number remains a constant value of 10. The effect of Carreau number on the drag coefficient is shown in Figure 6 while the power-law index is fixed at 0.4. As can be seen from Figure 6, when the Carreau number increases from 0.1 to 100, the effect of confining walls attenuates. In fact, this trend is very similar to that when the power law index decreases. The reason behind this phenomenon can be explained from Figure 2. When λ or Λ ($=\lambda V_0/d$) increases at a constant power-law index, n , the viscosity decreases. This effect can also be acquired by means of decreasing the power law index, n while the Carreau number keeps unchanged.

As done previously,^{2,3} to depict the role of n , Re and κ , drag coefficients in Carreau fluids



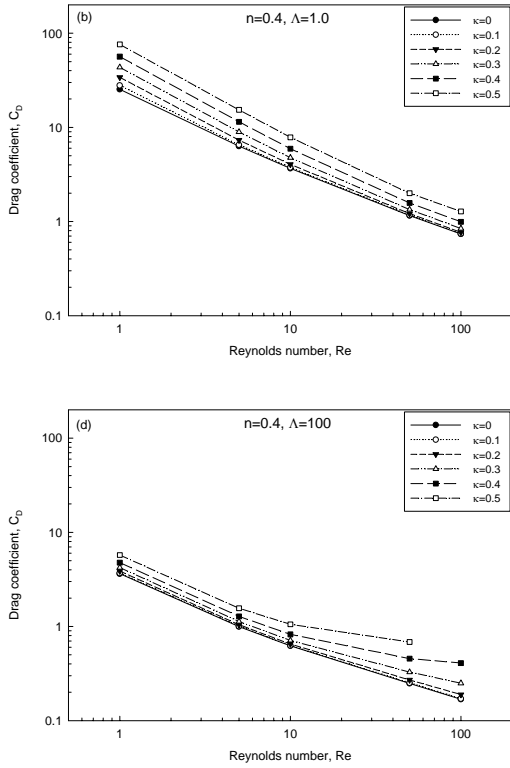


Figure 6. Dependence of drag coefficient on Carreau number, Λ at $n=0.4$. (a) $\Lambda=0.1$; (b) $\Lambda=1$; (c) $\Lambda=10$ [refer to Figure 5(d)]; and (d) $\Lambda=100$

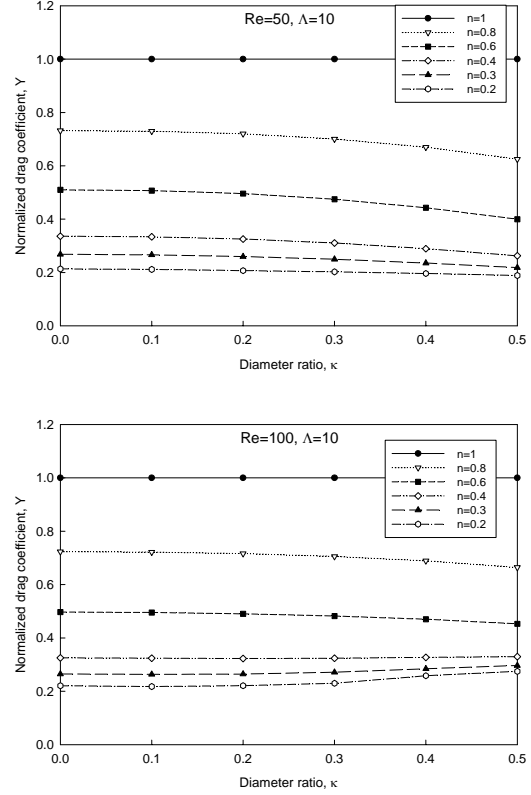
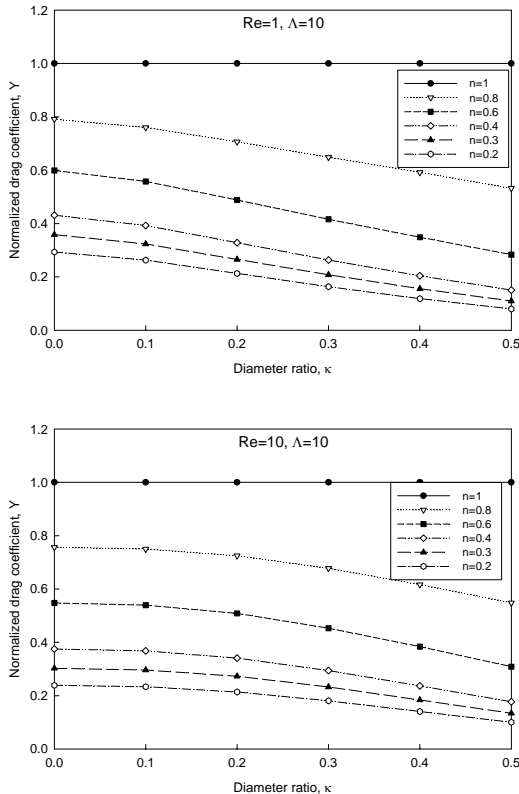


Figure 7. Dependence of normalized drag coefficient on Re , n and κ at $\Lambda=10$, (a) $Re=1$; (b) $Re=10$; (c) $Re=50$; (d) $Re=100$



fluids.² As shown in Figure 7 ($Re=100$), Y is insensitive to the diameter ratio under all shear-thinning scenarios.

4.3 Wake Characteristics

Velocity profile and streamline contours can give more insights into the detailed structure of the flow field. Generally, these are qualitatively similar to those reported in Ref. 2 and thus not shown here. For an unbounded case, the velocity field decays progressively from the vicinity of the sphere surface. Meanwhile, for a confined scenario, fluids are experienced increasing acceleration in the annular region, which indicates that fluids are subjected to higher shearing levels than other regions.² Combined with the shear-thinning behavior leads to a lower effective shear viscosity in this region, thereby increasing the local Reynolds number. Because this impact is augmented with the increasing degree of confinement and/or with the increasing extent of shear-thinning behavior, it is expected that the recirculation length should increase with the increase of κ and the decrease of n . At low Reynolds numbers, the flow remains attached to

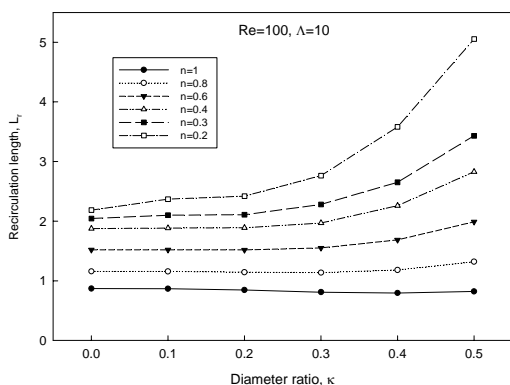


Figure 8. Effect of diameter ratio, κ and power law index, on the recirculation length at $Re=100$ and $\Lambda=10$

the sphere surface. When Re increases to some critical value ($\sim 20-24$ for a Newtonian fluid around an unbounded sphere), the flow will detach from the surface, thereby rendering the formation of recirculation in the rear of the sphere. Usually the wake characteristics are quantified in terms of the recirculation length, L_r measured from the rear of the sphere (non-dimensionalized using the sphere diameter) and the wake width, quantified by the separation angle, θ_s , measured from the front stagnation point of the sphere, where $\theta_s=0$. Figures 8 and 9 show typical results elucidating the effects of n and κ on L_r and θ_s at $Re=100$ and $\Lambda=10$. Indeed, Figure 8 reveals that the recirculation increases with the decrease of n and/or with the increase of κ . One also expects that the separation angle moves towards the front stagnation point, i.e., separation angle decreases when n decreases as shown in Figure 9. On the other hand, the wall effect on the separation angle is very limited, albeit the separation angle slightly moves towards the rear stagnation point with the confinement due to the suppression of the flow separation rendered by confining walls.

5. Conclusions

The governing equations for a rigid sphere falling in quiescent Carreau fluids in cylindrical tubes were numerically solved. The influence of Reynolds number, power law index, Carreau number and blockage ratio on the hydrodynamic drag on a sphere and wake were examined extensively. In general, due to the confining walls, the fluid in the annular region undergoes intense shearing and acceleration, thereby lowering the effective viscosity and raising the local Reynolds number. As a result, drag increases with the confining degree, but the wall

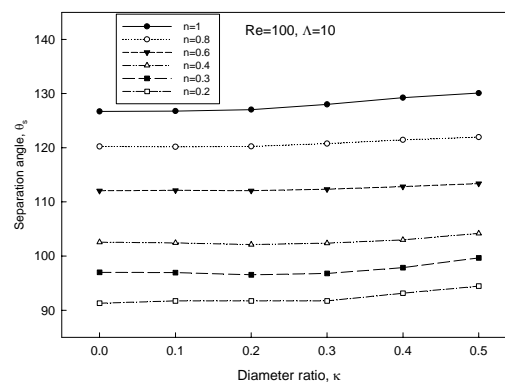


Figure 9. Effect of diameter ratio, κ and power law index, n on the separation angle at $Re=100$ and $\Lambda=10$

effect is less severe in Carreau fluids than that in Newtonian fluids and attenuates with Reynolds number. The shear-thinning behavior accentuates the recirculation length and the onset of separation. The severity of confining walls plays a less important role in affecting the wake characteristics. The numerical results herein are aligned with experimental data reported in the literature.

6. References

1. RP Chhabra, JF Richardson, *Non-Newtonian Flow and Applied Rheology*, 2nd ed., pp. 249-314, Oxford, Butterworth-Heinemann (2008)
2. D Song, RK Gupta, RP Chhabra, Wall effects on a sphere falling in quiescent power law fluids, *Ind. Eng. Chem. Res.*, **48**, 5845-5856 (2009)
3. D Song, RK Gupta, RP Chhabra, Drag on a sphere in Poiseuille flow of shear-thinning power-law fluids, *Ind. Eng. Chem. Res.*, in press, DOI: 10.1021/ie102120p (2011)
4. RP Chhabra, PHT Uhlherr, Creeping motion of spheres through shear-thinning elastic fluids described by the Carreau viscosity equation, *Rheol. Acta*, **19**, 187-195 (1980)
5. RP Chhabra, C Tiu, PHT Uhlherr, A study of wall effects on the motion of a sphere in viscoelastic fluids, *Can. J. Chem. Eng.* **59**, 771-775 (1981)
6. J Strnadel, M Simon, I Machač, Wall effects on terminal falling velocity of spherical particles moving in a Carreau model fluid, *Chem. Papers*, **65**, 177-184 (2011)
7. J-P Hsu, Y-H Hsieh, S Tseng, Drag force on rigid spheroidal particles in a cylinder filled with Carreau fluid, *J. Colloid Interface Sci.*, **284**, 729-741 (2005)
8. RB Bird, RC Armstrong, O Hassager, *Dynamic of Polymeric Liquid*, Vol. 1, 2nd ed., New York, Wiley (1987)